# A DNA Sensor Based on Upconversion Nanoparticles and 2D Dichalcogenide Materials

Konstantina Alexaki,[1, ‡] Davide Giust,[1, ‡] Maria-Eleni Kyriazi,[1] Afaf H. El-Sagheer,[2, 3] Tom Brown,[2] Otto L. Muskens,[1, 4] and Antonios G. Kanaras[1, 4*]

[1] School of Physics and Astronomy, Faculty of Engineering and Physical Sciences, University of Southampton, Southampton SO17 1BJ, UK.

[2] Department of Chemistry, University of Oxford, Chemistry Research Laboratory, 12 Mansfield Road, Oxford OX1 3TA, UK.

[3] Chemistry Branch, Department of Science and Mathematics, Faculty of Petroleum and Mining Engineering, Suez University, Suez 43721, Egypt.

[4] Institute for Life Sciences, University of Southampton, Southampton SO17 1BJ, UK.

*** Corresponding Author**

**Telephone: 0044 (0) 2380592466**

**Fax: 0044 (0) 2380593910**

E-mail: a.kanaras@soton.ac.uk

**Abstract**: We demonstrate the fabrication of a new DNA sensor that is based on the optical interactions occurring between oligonucleotide-coated $NaYF_4$: $Yb^{3+}$; $Er^{3+}$ upconversion nanoparticles and the 2D dichalcogenide materials, $MoS_2$ and $WS_2$. Monodisperse upconversion nanoparticles (27.4 ± 0.1 nm) were functionalized with single-stranded DNA endowing the nanoparticles with the ability to interact with the surface of the 2D materials *via* van der Waals interactions leading to subsequent quenching of the upconversion fluorescence. By contrast, in the presence of a complementary oligonucleotide target and the formation of double-stranded DNA, the upconversion nanoparticles could not interact with $MoS_2$ and $WS_2$, thus retaining their inherent fluorescence properties. Utilizing this sensor we were able to detect target oligonucleotides with high sensitivity and specificity whilst reaching a concentration detection limit as low as 5 fM, within minutes.

**Keywords**: upconversion nanoparticles, DNA, sensor, 2D materials, $MoS_2$, $WS_2$.

## Introduction

There is an ongoing interest towards the development of sensors for the detection of biomolecules.[1-4] Amongst various biomolecules, the detection of DNA and RNA has been of particular interest due to their involvement in a plethora of biological processes including gene regulation and protein production as well as various diseases such as cancer.[5-7]

Different types of biosensors have been designed capable of detecting DNA or RNA targets utilizing electrochemical, mass-based or optical methods.[8] For example, electrochemical sensors monitor variations in current in a solution containing the target.[9] While these sensors have significant advantages like durability, cheap thin-film applications, small-size dimensions and real-time monitoring, their weakness of being easily affected by temperature changes [10] and their lower sensitivity compared to other biosensors [11-12], limit their widespread availability. Surface acoustic wave sensors are mass-based biosensors that can detect acoustic waves generated by mass loading on their surface.[13] They represent a significant alternative for detection of biomolecules as they are rapid and label-free.[14] However, they present major disadvantages, which include mechanical instability and fragility.[15-16] Optical DNA or RNA sensors are based on the interaction of the optical field with nucleic acids.[17] They are broadly used because of their high sensitivity and specificity.[18] The most common types of optical sensors are: label-free systems that rely on plasmon resonance or optical resonance [19], and label-based systems involving the use of fluorophores, enzymes or nanoparticles.[20] Surface plasmon resonance (SPR) detection is based on the measurement of binding-induced refractive index changes in a sample region. This type of detection allows for quantitative and kinetic measurement of molecular interactions in real-time.[21] However, it is relatively challenging to develop SPR sensors for small molecules at low concentrations as the molecular weight of the target must be large enough to generate a measurable signal change.[22] Other common optical biosensors that involve the use of organic dyes, rely on the presence of an energy transfer pair in close proximity where the fluorescence of a donor is quenched by an acceptor - a process also called Förster Resonance Energy Transfer (FRET).[23] However, the use of organic dyes presents several limitations, such as the lack of stability due to photo-bleaching and photo-blinking.[24] Moreover, the typical photo-excitation of organic dyes in the UV-Vis region limits their use in complex biological environments due to the presence of undesired background autofluorescence deriving from proteins, cells and other biomolecules.[25]

To overcome the aforementioned obstacles, lanthanide doped upconversion nanoparticles (UCNPs) have emerged as reliable alternatives to standard organic fluorophores. The main characteristic of UCNPs is that they can convert near-infrared (NIR) light into visible light. The use of NIR excitation radiation enables penetration into biological samples more efficiently than visible light due to the optical transparent window of the electromagnetic spectrum in biological tissues.[26] UCNPs show high resistance to photo-bleaching or photo-blinking and they have narrow emissions in the visible area, which renders their fluorescent signal stable and easily detectable in multiplexing biosensors.[27-28] For these reasons, the production of highly efficient UCNPs is employed in a wide range of biological applications.[29-31]

An effective quencher for UCNPs is graphene oxide (GO). In previous studies, we have shown that UCNPs functionalized with single-stranded DNA (ssDNA) can adsorb to the GO surface *via* π-π staking generated interactions between the DNA strand and GO. Thus the close proximity of the UCNPs to the surface of GO resulted in the quenching of their fluorescence.[32] In contrast, double-stranded DNA (dsDNA) coated UCNPs did not interact with the GO surface as the nucleobases were efficiently shielded within the negatively charged phosphate backbone of dsDNA.[33] Thus, in the presence of the complementary oligonucleotide sequence the UCNPs did not adsorb to the GO surface retaining their fluorescence.[34] This methodology was utilized by us to construct sensors for the detection of mRNA-biomarkers, relevant to Alzheimer's disease and prostate cancer, in complex media such as blood plasma and cell lysate. Furthermore, we demonstrated the fabrication of a portable sensor for the field detection of mRNA-biomarkers related to crops' nutritional deficiencies.[35-36] Huang *et al*. also made a sensor for the detection of endonucleases using DNA-coated UCNPs and GO as a FRET pair. The resulting biosensor exhibited high sensitivity with a limit of detection of $1 \times 10^{-4}\ U\ mL^{-1}$ for S1 nuclease.[37]

Analogous materials as GO with special optical and electronic properties have recently been exploited for the fabrication of FRET assays. Two dimensional (2D) dichalcogenide materials have emerged as ideal energy transfer acceptors due to their large surface area, ease of synthesis of large single sheets and their increased affinity towards biomolecules. Luminescent 2D materials such as $MoS_2$ and $WS_2$ have also proven to be excellent quenchers in the area of optical biosensors.[38] SsDNA can adsorb onto the $MoS_2$ and $WS_2$ surface *via* van der Waals (vdW) forces rather than π-π staking interactions.[39] Liu's group studied the adsorption / desorption behavior of ssDNA with these materials by varying the ionic strength, the denaturing agents and the DNA length or sequence. They concluded, that compared to $MoS_2$ and $WS_2$, GO exhibited the highest affinity for DNA detection whilst the detection limit of these three sensors was quite similar when the same fluorescent DNA probe was used.[39] To greater extent, 2D materials are shown to be very good quenchers in the area of optical aptamer-based sensors. Recently, Kenry and co-workers presented the fluorescence detection of a highly expressed malarial biomarker, *Plasmodium* lactose dehydrogenase (pLDH) protein, by using single-layer $MoS_2$ nanosheets and single stranded aptamer probe labeled with the fluorescent dye, fluorescein (FAM). This aptamer-nanosheet sensing platform was capable of distinguishing the target pLDH protein in a heterogeneous mixture of proteins.[40] Lv *et al.* developed a strategy for the detection of microcystin-LR, a representative toxin released by cyanobacteria in water, using DNA-coated UCNPs and $MoS_2$. This aptamer-based sensor was proven to work efficiently even in 'real' samples such as tap and lake water.[41] An aptamer-based sensor was also developed by Yuan *et al.*. Their study focused on the use of $MoS_2$ and UCNPs as a FRET pair for the detection of the tumor marker $VEGF_{165}$.[42]

In this work, we show how $MoS_2$ and $WS_2$ can be utilized for sensing of a synthetic oligonucleotide target. We demonstrate the detection of a poly-A DNA target in phosphate buffer saline (PBS) by exploiting the interactions occurring between ssDNA-coated UCNPs and $MoS_2$ / $WS_2$ in solution. **Scheme 1** depicts the working mechanism of the biosensor. In the presence of $MoS_2$ or $WS_2$, the ssDNA-coated UCNPs adsorb onto the surface of the dichalcogenide resulting in fluorescence quenching of the UCNPs. However, when the complementary DNA sequence is present the dsDNA-coated UCNPs do not adsorb onto the dichalcogenide surface thus retaining their fluorescent

signal. On the other hand, in the presence of a non-complementary sequence, the fluorescence of the UCNPs is quenched and no fluorescent signal is detected, demonstrating the specificity of the sensor.

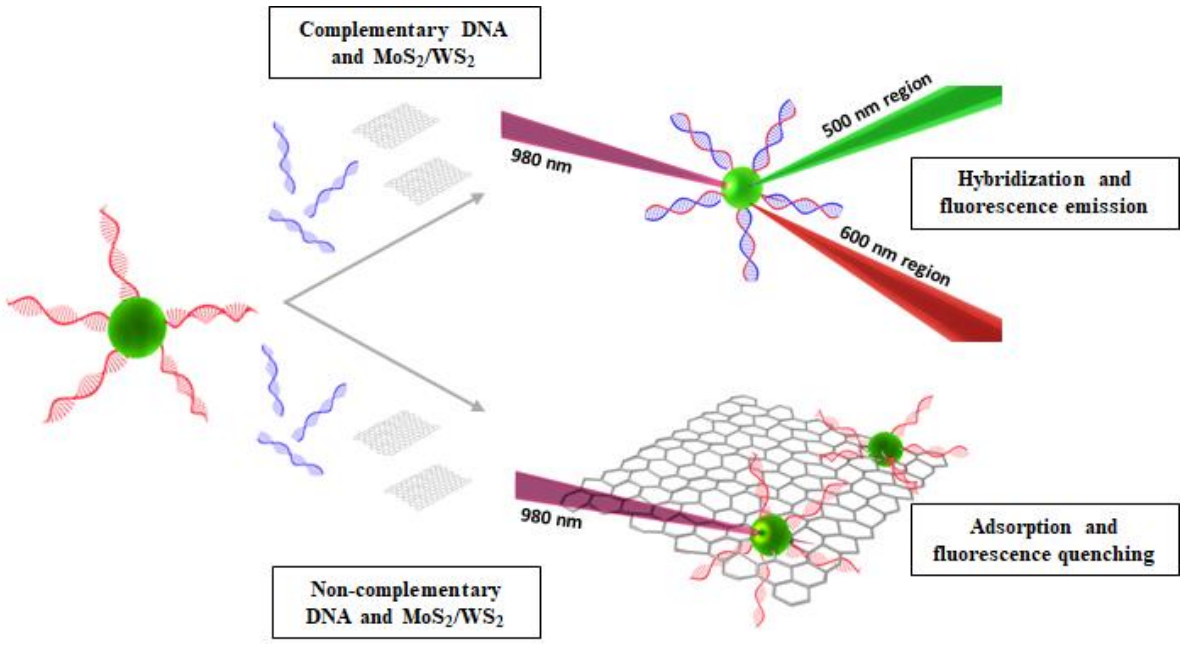


**Scheme 1.** Schematic illustration presenting the working principle of the DNA sensor. In the absence of a complementary DNA target, $MoS_2$ and $WS_2$ quench the UCNP emitted fluorescence. When hybridized to the complementary DNA target, the dsDNA-coated UCNPs do not adsorb to the surface of the dichalcogenides and therefore their fluorescence is retained.

## Results and Discussion

### Synthesis and Characterization of oligonucleotide functionalized UCNPs.

In order to investigate the interactions occurring between ssDNA-coated UCNPs and $MoS_2$ / $WS_2$, we firstly synthesized hexagonal phase $NaYF_4$: $Yb^{3+}$ (18%); $Er^{3+}$ (2%) @ $NaYF_4$ core-shell NPs based on a modified solvothermal method.[43] Our synthesis yielded highly monodisperse hexagonal shaped core-shell UCNPs with an average nanocrystal size of 27.4 ± 0.1 nm (see **Figure S1**). XRD measurements confirmed that the hexagonal phase of the UCNPs was retained after core-shell formation (see **Figure S2**). The presence of the $NaYF_4$ shell accounted for a decrease of defects on the UCNPs crystal surface thus improving their fluorescent emission in water where the upconversion processes can be strongly affected by vibrational scattering of water molecules adsorbed onto the crystal surface.[44-45] Following our previously established protocols, a ligand exchange procedure was further performed where the original oleic acid ligands on the UCNP surface were replaced by poly-acrylic acid (PAA) to enable nanoparticle solubility in water and further facilitate their functionalization with

amino-modified ssDNA sequences.[35-36] An EDC coupling reaction was utilized in order to attach the amino-modified synthetic oligonucleotides to the carboxylic group of the PAA ligands on the UCNPs surface. The successful coupling was firstly confirmed by zeta potential measurements where a decrease in the net charge was observed (see **Figure S4**) and FT-IR analysis where the characteristic peak of the carboxyl group of the PAA disappeared (see **Figure S5**).

**Quenching of UCNPs' fluorescence by $MoS_2$ and $WS_2$.**

Following successful synthesis and characterization of ssDNA-coated UCNPs we evaluated the ability of $MoS_2$ and $WS_2$ (see **Figure S6** for characterization of $MoS_2$ and $WS_2$) to quench the emission of the functionalized NPs. **Figure 1** shows the recorded fluorescence spectra of ssDNA-coated UCNPs (0.5 $mg{\cdot}mL^{-1}$) in the presence of various concentrations of $MoS_2$ and $WS_2$. Upon increasing concentrations of 2D materials, whilst maintaining the same concentration of ssDNA-coated UCNPs (0.5 $mg{\cdot}mL^{-1}$), a steady decrease in the fluorescence intensity of the UCNPs was observed. This is a strong indication that the interactions between the 2D materials and ssDNA-coated UCNPs were within the distance required for a nonradiative energy transfer, which resulted in fluorescence quenching.[46]

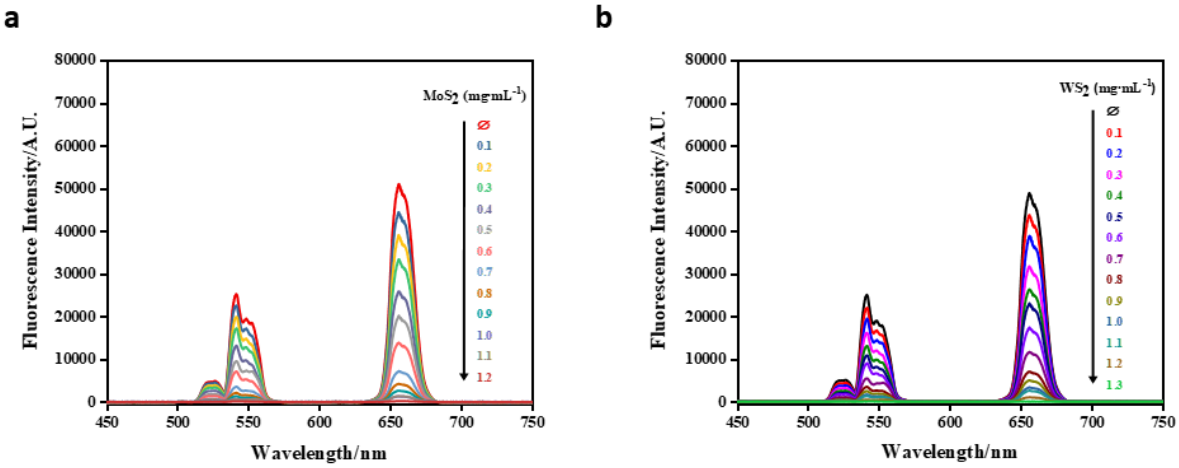


**Figure 1.** Representative fluorescence emission spectra from ssDNA-coated UCNPs (0.5 $mg{\cdot}mL^{-1}$) in the presence of increasing concentrations of $MoS_2$ (**a**) or $WS_2$ (**b**).

To further investigate the nature of the interactions occurring between the ssDNA-coated UCNPs and the 2D dichalcogenides we correlated the intensity at lambda max for each UCNP emission peak observed in the fluorescence spectra with the quenching ability of $MoS_2$ and $WS_2$. **Figure 2** shows the analysis of fluorescence quenching of ssDNA-coated UCNPs at wavelengths of 540 and 655 nm as a function of $MoS_2$ and $WS_2$ concentration. Indeed, a quenching ability of more than 94% was observed upon addition of 1.2 $mg{\cdot}mL^{-1}$ of $MoS_2$ and 1.3 $mg{\cdot}mL^{-1}$ of $WS_2$ respectively. This degree of quenching correlates well with the quenching effect previously observed for GO against the UCNPs' emitted fluorescence as a result of the FRET process occurring between the donor (UCNPs) and the acceptor (2D material).[34, 46] In this study, the UCNPs fluorescence quenching followed the same trend, which indicates that this quenching is due to a FRET process.

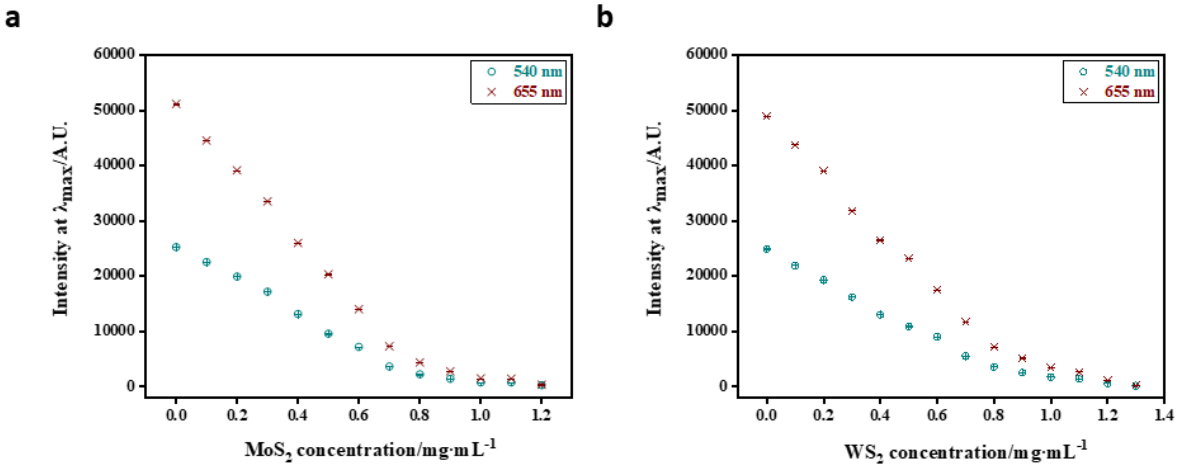


**Figure 2.** Correlated fluorescence emission spectra from ssDNA-coated UCNPs (0.5 mg·mL$^{-1}$) showing the decreasing fluorescence emission of the $\lambda_{max}$ of the two typical peaks of UCNPs (655 nm, red points; 540 nm, cyan points) in the presence of increasing concentration of $MoS_2$ (**a**) or $WS_2$ (**b**) as indicated in the graph.

**Oligonucleotide target detection.**

In order to fully investigate the ability of ssDNA-coated UCNPs to induce an interaction with the chosen 2D materials we incubated $MoS_2$ and $WS_2$, at concentrations previously determined to induce the most effective quenching with functionalized UCNPs. **Figure 2** shows that the distinct fluorescence emission of UCNPs was significantly quenched when coated with a monolayer of ssDNA indicating that the main driving forces rely on vdW interactions between the ssDNA and the 2D surface as also reported by others.[39, 46] To further investigate the presence of such interactions, ssDNA-coated UCNPs were hybridized to their complementary sequences (see Table S1 for oligonucleotide sequences) and then $MoS_2$ or $WS_2$ were added. **Figure 3** shows results obtained upon hybridization with an increasing concentration of complementary target (cDNA) for 30 minutes. As the concentration of the target was increased from 5 fM to 50 nM, a decrease in the quenching efficiency of $MoS_2$ (**Figure 3 a**) and $WS_2$ (**Figure 3 b**) over both characteristic peaks was observed. This is due to the conformational change taking place upon DNA duplex formation, which prevented adsorption of the dsDNA-coated UCNPs onto the $MoS_2$ or $WS_2$ surface thus retaining their fluorescence properties.

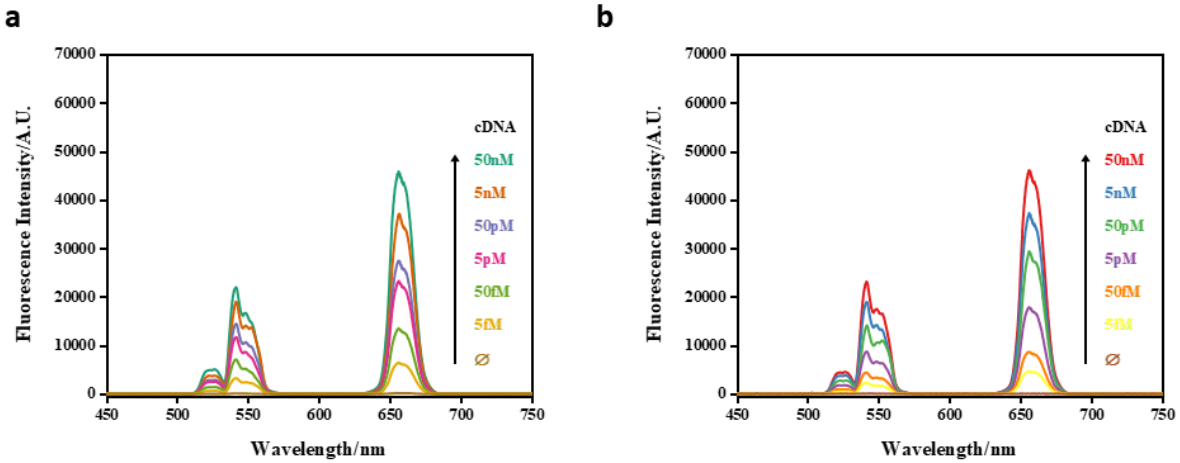


**Figure 3.** Representative fluorescence spectra of ssDNA-coated UNCPs (0.5 mg·mL$^{-1}$) in the presence of increasing concentrations of complementary DNA targets for $MoS_2$ (**a**) and $WS_2$ (**b**).

**Figure 4** shows the maximum intensity recorded for each peak at wavelengths of 540 and 655 nm as a function of the target concentration. By plotting a semi-log graph, a trend was observed where a pronounced effect in fluorescence recovery was observed at a concentration of 50 pM and 5 nM for $MoS_2$ (**Figure 4 a**) and $WS_2$ (**Figure 4 b**) respectively. For lower target concentrations, fluorescence recovery was less efficient due to potential lower number of hybridization events occurring. Thus quenching by $MoS_2$ and $WS_2$ due to adsorption of ssDNA-coated UCNPs onto the surface was still observed at such cDNA concentrations demonstrating that fluorescence intensity is dependent on target detection.

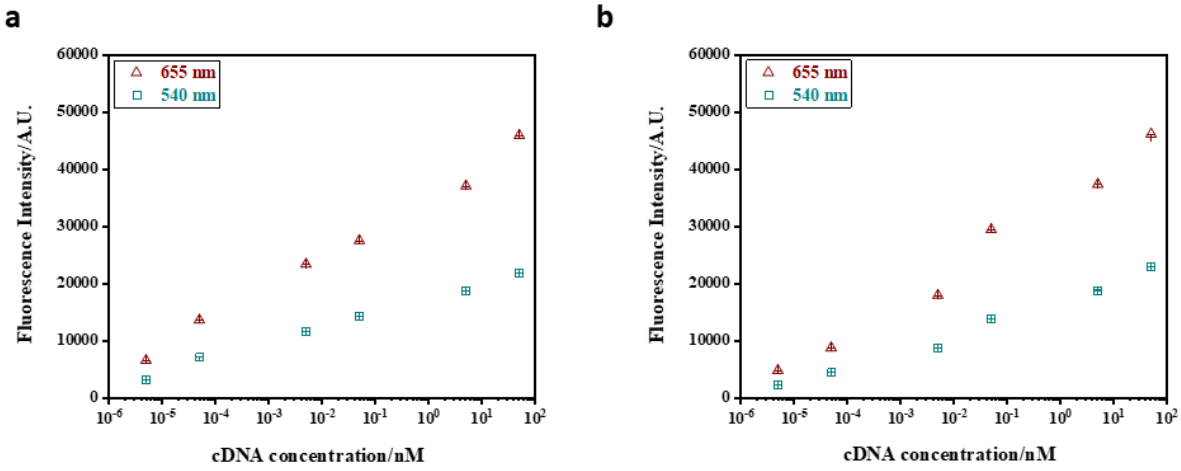


**Figure 4.** Graphs of the maximum nanoparticle fluorescence intensity bands measured at 540 nm and 655 nm for $MoS_2$ (**a**) and $WS_2$ (**b**) as a function of cDNA concentration.

The specificity of this system was further confirmed by performing a control experiment where ssDNA-coated UCNPs (0.5 mg·mL$^{-1}$) were incubated with a non-complementary target sequence prior to addition of $MoS_2$ and $WS_2$. **Figure 5** shows the fluorescence emission spectra recorded following incubation with DNA concentrations

ranging from 5 to 1000 nM. In both cases no fluorescence was observed (**Figure 5**) regardless of the concentration of the non-complementary DNA target initially added. This indicated the predominant existence of ssDNA on the UCNP surface, which permitted their adsorption onto the surface of $MoS_2$ or $WS_2$ respectively, thus rendering their fluorescence quenched.

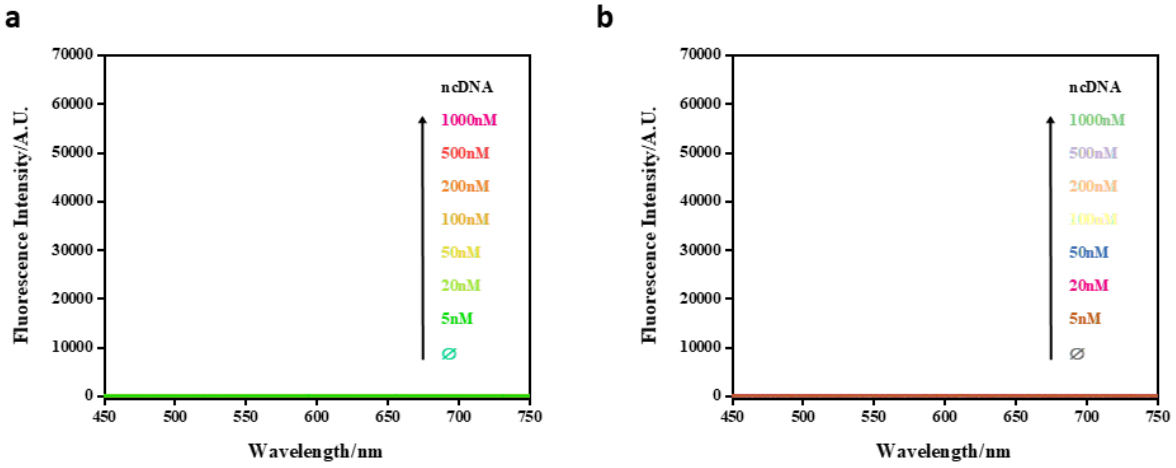


**Figure 5.** Fluorescence spectra of ssDNA-coated UCNPs (0.5mg·mL$^{-1}$) in the presence of various concentrations of the non-complementary target for 1.2 mg·mL$^{-1}$ $MoS_2$ (**a**) and 1.3 mg·mL$^{-1}$ $WS_2$ (**b**).

## Conclusions

In summary, we showed the development and use of an optical DNA sensor made from ssDNA-coated UCNPs and 2D dichalcogenides ($MoS_2$ and $WS_2$). The well-developed concept of a sensor, which combines the emissive properties of UCNPs and the quenching ability of GO, has been herein implemented by considering alternative 2D materials. The working principle of the sensor is based on the property of dichalcogenides to adsorb ssDNA to their surface *via* vdW interactions. In the absence of a target DNA, ssDNA-coated UCNPs were adsorbed onto the surface of $MoS_2$ or $WS_2$ and their fluorescence was quenched. In the presence of a complementary target DNA hybridized to the oligonucleotides on the surface of the UCNPs, the particles could no longer adsorb to the surface of the dichalcogenides and their fluorescence was retained. Utilizing this sensor, we were able to detect target DNAs within few minutes at the 5fM range. Our results pave the way towards the development of oligonucleotide sensors for related biomedical applications. Future research could also involve other dichalcogenide such as $TaS_2$ and $TiS_2$, which have already been found to serve as suitable energy transfer acceptors upon their interaction with dye-modified oligonucleotides.[47]

## Materials and Methods

**Materials.** All chemical reagents were used as received without further purification and were obtained from commercial sources. Yttrium(III) chloride hexahydrate (98%), ytterbium(III) chloride hexahydrate (99.9%), erbium(III) chloride hexahydrate (99.9%),

ammonium fluoride (98%), methanol (99.9%), n-hexane (95%), poly(acrylic acid) (PAA) (MW≈1.8 kDa), phosphate buffered saline tablets (PBS), 2-(N-Morpholino) ethanesulfonic acid, 4-Morpholineethanesulfonic acid (MES), sodium borate, sodium chloride, 1-octadecene (90%), oleic acid (90%), N-(3-(dimethylamino)propyl)-N'-ethylcarbodiimide hydrochloride (EDC) (99%) and N-hydroxysulfosuccinimide sodium salt (Sulfo-NHS) (98%) were purchased from Merck. Tetrahydrofuran (THF), ethanol and hexane were purchased from Thermo Fisher Scientific in laboratory grade. $MoS_2$ and $WS_2$ (black powders of monolayer sheets dispersed in PBS before use) were purchased from ACS Material. $MoS_2$ monolayers exhibit a diameter between 1-3 μm, with a thickness of ~1 nm and a monolayer ratio ≥ 90% while $WS_2$ monolayers exhibit a diameter between 0.1-4 μm, a thickness of ~1 nm and a monolayer ratio of ≥ 90%.

**Methods.** Transmission Electron Microscopy (TEM) samples were prepared by depositing a drop of a diluted nanoparticle solution on a 400 mesh formvar coated copper grid and left in air to dry. Nanoparticles were observed on a Hitachi HT7700 TEM operating at an accelerating voltage of 100 kV. The size distribution of the core-shell UCNPs after annealing treatment was determined to be 27.4 ± 0.1 nm by counting over 200 nanoparticles using ImageJ software (National Institutes of Health, U.S.A.). The upconversion fluorescence measurements were performed using an aligned setup which consisted of a 300 mW, 980 nm diode laser (Thorlabs LTD, U.K.) as an excitation source and a short pass IR-blocking filter (Schott KG3) in order to suppress scattered excitation light and select only the fluorescence emission. The detector was a SpectraSuite Spectrometer (OceanOptics, U.S.A.) where the emitted fluorescence was collected perpendicular to the excitation beam using a 35 mm focal length lens. By illuminating a cuvette filled with the appropriate solvent with the same laser beam, the blank for each measurement was determined. All measurements were performed under 1000 ms of integration time and 10 scans to average. The fluorescent experiments were repeated three times and the fitted data corresponded to the mean value ± standard error of the mean (SEM).

**Synthesis of core UCNPs.** The synthesis of core UCNPs was carried out following a published protocol with some modifications.[48] The rare earth salts, $YCl_3 \cdot 6H_2O$ (236 mg, 0.78 mmol), $YbCl_3 \cdot 6H_2O$ (77.5 mg, 0.20 mmol), and $ErCl_3 \cdot 6H_2O$ (7.63 mg, 0.02 mmol) were put in a 100 mL round-bottom flask together with 6 mL of oleic acid and 15 mL of 1-octadecene. The solution was heated up to 150 °C under the presence of Ar flow and left at this temperature for 1 h and 30 min. Then, the reaction mixture was cooled down to room temperature. A solution of NaOH (100 mg, 2.5 mmol) and $NH_4F$ (148.16 mg, 4 mmol) dissolved in 10 mL of dry MeOH was injected dropwise to the reaction mixture under vigorous stirring. After 45 min of stirring at room temperature, the solution was gradually heated up to 100 $^oC$ under Ar for an additional 30 min to assist with the evaporation of MeOH. Then, the reaction mixture was stirred under vacuum for 30 min in order to ensure the complete evaporation of the MeOH. After, the temperature was increased at 310 $^oC$ under Ar and the solution was left under stirring for 1h 20 min to form the particles. Finally, the particles were left to cool down to room temperature. The solution was rinsed with EtOH (20 mL) and centrifuged (5,000 rpm, 15 min) three times for particles' purification. Each time UCNPs were re-dispersed in EtOH (20 mL). The nanoparticles' pellet was left to dry for several hours, weighted and stored for further experiments.

**Synthesis of core-shell UCNPs.** The synthesis of core-shell nanocrystals was performed based on a previously published protocol with some modifications.[49] In more detail, $YCl_3 \cdot 6H_2O$ (151.68 mg, 0.5 mmol) was dissolved in a solution of 1-octadecene (15 mL) and oleic acid (6 mL) and stirred for 1h under Ar at 150 $^oC$. The solution was left to cool down to 80 $^oC$ under a steady flow of Ar. A solution of core UCNPs (125 mg) dissolved in $CHCl_3$ (10 mL) was injected dropwise. The solution was gradually heated up to 100 $^oC$ under Ar flow for 20 min. Then, the mixture was left to cool down at room temperature under Ar. A solution of NaOH (50 mg, 1.25 mmol) and $NH_4F$ (74.08 mg, 2 mmol) dissolved in dry MeOH (5 mL) was added dropwise to the reaction mixture and was stirred for other 45 min. Afterwards, the temperature increased gradually up to 130 $^oC$ under Ar and the solution was stirred for 30 min. For ensuring the complete evaporation of MeOH, it was stirred for other 30 min at 130 $^oC$ under vacuum. Finally, the temperature was increased at 310 $^oC$ under Ar and the mixture was left under stirring for 1 h 20 min to form the core-shell particles. After completion of the reaction, the nanoparticles were left to cool down to room temperature. The solution was rinsed with EtOH (20 mL) and centrifuged (5,000 rpm, 15 min) three times in order to purify the particles. Each time UCNPs were re-dispersed in EtOH (20 mL). The core-shell UCNPs' pellet was collected and re-dispersed in THF.

**Ligand exchange on core-shell UCNPs.** A ligand exchange protocol was followed to coat the nanoparticle surface with poly-acrylic-acid (PAA) in order to bring the UCNPs in water.[50] A solution of PAA (0.25 g, MW ≈ 1.8 KDa) dissolved in THF (3 mL) was added to the core-shell UCNPs coated with oleic acid and re-dispersed in 7mL THF. The mixture was left stirring for 48 h at room temperature to allow the ligand exchange to happen. The final solution was centrifuged (5,000 rpm, 15 min) and washed with EtOH (20 mL) twice. The particles' pellet was dried and re-suspended in sterile DNAse / RNAse free Milli-Q water and stored at 4 $^oC$.

**Synthesis and characterizations of ssDNA PAA coated core-shell UCNPs.** The amino-modified oligonucleotides were covalently attached to the surface of the PAA coated core-shell UCNPs *via* the carboxylic groups on the PAA ligand using EDC amino-coupling chemistry. A solution of EDC (20 μL, 0.3 M) and sulfo-NHS (20 μL, 0.3 M) in MES buffer (pH 5.5, 0.1 M) was added to PAA coated core-shell UCNPs (0.5 $mg \cdot mL^{-1}$) suspended in borate buffer (pH 8.5, 0.01 M). The mixture was sonicated (10 min) thus the desired amino-terminated oligonucleotide sequence was added (poly-T, 22 μL, 236 μM). The reaction was stirred overnight, and the particles were purified by centrifugation (16,400 rpm, 4 $^oC$, 10 min) three times. The functionalized with ssDNA core-shell UCNPs were re-suspended in PBS and stored at 4 $^oC$.

**Sensor calibration.** In order to accurately calibrate the sensor, increasing concentrations of 2D materials (0.1 – 1.3 $mg \cdot mL^{-1}$) were added to a solution containing a fixed concentration of functionalized UCNPs (0.5 $mg \cdot mL^{-1}$) dispersed in PBS. The corresponding fluorescence spectra of the DNA-coated UCNPs were monitored in order to determine the concentration of the 2D materials that would results in optimum fluorescence quenching.

**Targeted DNA detection using DNA-coated UCNPs.** In order to prevent the interaction between the ssDNA-coated UCNPs and the 2D materials, the ssDNA was hybridized with its complementary sequence before incubating with the 2D material. To this purpose, 0.5 $mg \cdot mL^{-1}$ of ssDNA-coated UCNPs were incubated in PBS with various

concentrations of the complementary DNA strand (ranging from 5 fM to 50 nM) overnight while shaking. After this, a solution of $MoS_2$ or $WS_2$ dispersed in PBS was added and left incubating for 10 min prior to performing the fluorescence measurements.

## Electronic Supplementary Material

Supplementary material is available in the online version of this article.

Raw data of this work is available at https://doi.org/10.5258/SOTON/D1553.

## Author Contributions

All authors have given approval to the final version of the manuscript. ‡These authors contributed equally.

## Acknowledgments

AGK, OLM and DG would like to acknowledge funding from BBSRC (BB/N021150/1). AK would like to thank the University of Southampton for a Mayflower PhD studentship.

## References

1. Wang, J., DNA biosensors based on peptide nucleic acid (PNA) recognition layers. A review. Biosensors & Bioelectronics 1998, 13 (7-8), 757-762.
2. Leatherbarrow, R. J.; Edwards, P. R., Analysis of molecular recognition using optical biosensors. Current Opinion in Chemical Biology 1999, 3 (5), 544-547.
3. Akyilmaz, E.; Yorganci, E.; Asav, E., Do copper ions activate tyrosinase enzyme? A biosensor model for the solution. Bioelectrochemistry 2010, 78 (2), 155-160.
4. Soraya, G. V.; Chan, J. X.; Nguyen, T. C.; Huynh, D. H.; Abeyrathne, C. D.; Chana, G.; Todaro, M.; Skafidas, E.; Kwan, P., An interdigitated electrode biosensor platform for rapid HLA-B*15:02 genotyping for prevention of drug hypersensitivity. Biosensors and Bioelectronics 2018, 111, 174-183.
5. Contag, C. H.; Bachmann, M. H., Advances in in vivo bioluminescence imaging of gene expression. Annu Rev Biomed Eng 2002, 4, 235-60.
6. Heuer-Jungemann, A.; El-Sagheer, A. H.; Lackie, P. M.; Brown, T.; Kanaras, A. G., Selective killing of cells triggered by their mRNA signature in the presence of smart nanoparticles. Nanoscale 2016, 8 (38), 16857-16861.
7. Halo, T. L.; McMahon, K. M.; Angeloni, N. L.; Xu, Y.; Wang, W.; Chinen, A. B.; Malin, D.; Strekalova, E.; Cryns, V. L.; Cheng, C.; Mirkin, C. A.; Thaxton, C. S., NanoFlares for the detection, isolation, and culture of live tumor cells from human blood. Proc. Natl. Acad. Sci. U.S.A. 2014, 111 (48), 17104-17109.
8. Mobed, A.; Hasanzadeh, M.; Ahmadalipour, A.; Fakhari, A., Recent advances in the biosensing of neurotransmitters: material and method overviews towards the biomedical analysis of psychiatric disorders. Analytical Methods 2020, 12 (4), 557-575.

9. Blair, E. O.; Corrigan, D. K., A review of microfabricated electrochemical biosensors for DNA detection. Biosensors and Bioelectronics 2019, 134, 57-67.
10. Mehrvar, M.; Abdi, M., Recent developments, characteristics, and potential applications of electrochemical biosensors. Analytical Sciences 2004, 20 (8), 1113-1126.
11. Matharu, Z.; Daggumati, P.; Wang, L.; Dorofeeva, T. S.; Li, Z. D.; Seker, E., Nanoporous-Gold-Based Electrode Morphology Libraries for Investigating Structure-Property Relationships in Nucleic Acid Based Electrochemical Biosensors. Acs Applied Materials & Interfaces 2017, 9 (15), 12959-12966.
12. Garcia, T.; Revenga-Parraa, M.; Anorga, L.; Arana, S.; Pariente, F.; Lorenzo, E., Disposable DNA biosensor based on thin-film gold electrodes for selective Salmonella detection. Sensors and Actuators B-Chemical 2012, 161 (1), 1030-1037.
13. Lange, K.; Rapp, B. E.; Rapp, M., Surface acoustic wave biosensors: a review. Analytical and Bioanalytical Chemistry 2008, 391 (5), 1509-1519.
14. Ten, S. T.; Hashim, U.; Gopinath, S. C. B.; Liu, W. W.; Foo, K. L.; Sam, S. T.; Rahman, S. F. A.; Voon, C. H.; Nordin, A. N., Highly sensitive Escherichia coli shear horizontal surface acoustic wave biosensor with silicon dioxide nanostructures. Biosensors and Bioelectronics 2017, 93, 146-154.
15. Zhang, Y. L.; Yang, F.; Sun, Z. Y.; Li, Y. T.; Zhang, G. J., A surface acoustic wave biosensor synergizing DNA-mediated in situ silver nanoparticle growth for a highly specific and signal-amplified nucleic acid assay. Analyst 2017, 142 (18), 3468-3476.
16. Afzal, A.; Mujahid, A.; Schirhagl, R.; Bajwa, S. Z.; Latif, U.; Feroz, S., Gravimetric Viral Diagnostics: QCM Based Biosensors for Early Detection of Viruses. Chemosensors 2017, 5 (1).
17. Damborsky, P.; Svitel, J.; Katrlik, J., Optical biosensors. Biosensor Technologies for Detection of Biomolecules 2016, 60 (1), 91-100.
18. Dey, D.; Goswami, T., Optical Biosensors: A Revolution Towards Quantum Nanoscale Electronics Device Fabrication. Journal of Biomedicine and Biotechnology 2011.
19. Shin, Y.; Perera, A. P.; Park, M. K., Label-free DNA sensor for detection of bladder cancer biomarkers in urine. Sensors and Actuators B-Chemical 2013, 178, 200-206.
20. Petty, J. T.; Story, S. P.; Hsiang, J. C.; Dickson, R. M., DNA-Templated Molecular Silver Fluorophores. Journal of Physical Chemistry Letters 2013, 4 (7), 1148-1155.
21. Nguyen, H. H.; Park, J.; Kang, S.; Kim, M., Surface Plasmon Resonance: A Versatile Technique for Biosensor Applications. Sensors 2015, 15 (5), 10481-10510.
22. Patil, P. O.; Pandey, G. R.; Patil, A. G.; Borse, V. B.; Deshmukh, P. K.; Patil, D. R.; Tade, R. S.; Nangare, S. N.; Khan, Z. G.; Patil, A. M.; More, M. P.; Veerapandian, M.; Bari, S. B., Graphene-based nanocomposites for sensitivity enhancement of surface plasmon resonance sensor for biological and chemical sensing: A review. Biosensors and Bioelectronics 2019, 139.
23. Shi, J. Y.; Tian, F.; Lyu, J.; Yang, M., Nanoparticle based fluorescence resonance energy transfer (FRET) for biosensing applications. Journal of Materials Chemistry B 2015, 3 (35), 6989-7005.
24. Schuster, J.; Brabandt, J.; von Borczyskowski, C., Discrimination of photoblinking and photobleaching on the single molecule level. Journal of Luminescence 2007, 127 (1), 224-229.
25. Frangioni, J. V., In vivo near-infrared fluorescence imaging. Curr Opin Chem Biol 2003, 7 (5), 626-34.
26. Smith, A. M.; Mancini, M. C.; Nie, S. M., BIOIMAGING Second window for in vivo imaging. Nature Nanotechnology 2009, 4 (11), 710-711.

27. Binnemans, K., Lanthanide-based luminescent hybrid materials. Chem Rev 2009, 109 (9), 4283-374.
28. Wang, X.; Valiev, R. R.; Ohulchanskyy, T. Y.; Agren, H.; Yang, C.; Chen, G., Dye-sensitized lanthanide-doped upconversion nanoparticles. Chem Soc Rev 2017, 46 (14), 4150-4167.
29. Wang, Y. F.; Liu, G. Y.; Sun, L. D.; Xiao, J. W.; Zhou, J. C.; Yan, C. H., Nd(3+)-sensitized upconversion nanophosphors: efficient in vivo bioimaging probes with minimized heating effect. Acs Nano 2013, 7 (8), 7200-6.
30. Liu, J.; Liu, Y.; Bu, W.; Bu, J.; Sun, Y.; Du, J.; Shi, J., Ultrasensitive nanosensors based on upconversion nanoparticles for selective hypoxia imaging in vivo upon near-infrared excitation. Journal of the American Chemical Society 2014, 136 (27), 9701-9.
31. Chen, Z.; Chen, H.; Hu, H.; Yu, M.; Li, F.; Zhang, Q.; Zhou, Z.; Yi, T.; Huang, C., Versatile synthesis strategy for carboxylic acid-functionalized upconverting nanophosphors as biological labels. Journal of the American Chemical Society 2008, 130 (10), 3023-9.
32. Huang, Y. X.; Shi, Y. M.; Yang, H. Y.; Ai, Y., A novel single-layered MoS2 nanosheet based microfluidic biosensor for ultrasensitive detection of DNA. Nanoscale 2015, 7 (6), 2245-2249.
33. Wu, M.; Kempaiah, R.; Huang, P. J. J.; Maheshwari, V.; Liu, J. W., Adsorption and Desorption of DNA on Graphene Oxide Studied by Fluorescently Labeled Oligonucleotides. Langmuir 2011, 27 (6), 2731-2738.
34. Alonso-Cristobal, P.; Vilela, P.; El-Sagheer, A.; Lopez-Cabarcos, E.; Brown, T.; Muskens, O. L.; Rubio-Retama, J.; Kanaras, A. G., Highly Sensitive DNA Sensor Based on Upconversion Nanoparticles and Graphene Oxide. ACS Appl Mater Interfaces 2015, 7 (23), 12422-9.
35. Vilela, P.; El-Sagheer, A.; Millar, T. M.; Brown, T.; Muskens, O. L.; Kanaras, A. G., Graphene Oxide-Upconversion Nanoparticle Based Optical Sensors for Targeted Detection of mRNA Biomarkers Present in Alzheimer's Disease and Prostate Cancer. ACS Sens 2017, 2 (1), 52-56.
36. Giust, D.; Lucio, M. I.; El-Sagheer, A. H.; Brown, T.; Williams, L. E.; Muskens, O. L.; Kanaras, A. G., Graphene Oxide-Upconversion Nanoparticle Based Portable Sensors for Assessing Nutritional Deficiencies in Crops. Acs Nano 2018, 12 (6), 6273-6279.
37. Huang, L. J.; Tian, X.; Yi, J. T.; Yu, R. Q.; Chu, X., A turn-on upconversion fluorescence resonance energy transfer biosensor for ultrasensitive endonuclease detection. Analytical Methods 2015, 7 (18), 7474-7479.
38. Wang, F. F.; Qu, X. T.; Liu, D. X.; Ding, C. P.; Zhang, C. L.; Xian, Y. Z., Upconversion nanoparticles-MoS2 nanoassembly as a fluorescent turn-on probe for bioimaging of reactive oxygen species in living cells and zebrafish. Sensors and Actuators B-Chemical 2018, 274, 180-187.
39. Lu, C.; Liu, Y. B.; Ying, Y. B.; Liu, J. W., Comparison of MoS2, WS2, and Graphene Oxide for DNA Adsorption and Sensing. Langmuir 2017, 33 (2), 630-637.
40. Kenry; Geldert, A.; Zhang, X.; Zhang, H.; Lim, C. T., Highly Sensitive and Selective Aptamer-Based Fluorescence Detection of a Malarial Biomarker Using Single-Layer MoS2 Nanosheets. Acs Sensors 2016, 1 (11), 1315-1321.
41. Lv, J. J.; Zhao, S.; Wu, S. J.; Wang, Z. P., Upconversion nanoparticles grafted molybdenum disulfide nanosheets platform for microcystin-LR sensing. Biosensors and Bioelectronics 2017, 90, 203-209.

42. Yuan, Y.; Yu, H.; Yin, Y., A highly sensitive aptasensor for vascular endothelial growth factor based on fluorescence resonance energy transfer from upconversion nanoparticles to MoS2 nanosheets. Analytical methods : advancing methods and applications 2020.
43. Wang, M.; Abbineni, G.; Clevenger, A.; Mao, C. B.; Xu, S. K., Upconversion nanoparticles: synthesis, surface modification and biological applications. Nanomedicine-Nanotechnology Biology and Medicine 2011, 7 (6), 710-729.
44. Huang, X. Y.; Lin, J., Active-core/active-shell nanostructured design: an effective strategy to enhance Nd3+/Yb3+ cascade sensitized upconversion luminescence in lanthanide-doped nanoparticles. Journal of Materials Chemistry C 2015, 3 (29), 7652-7657.
45. Nie, Z. Y.; Ke, X. X.; Li, D. N.; Zhao, Y. L.; Zhu, L. L.; Qiao, R.; Zhang, X. L., NaYF4:Yb,Er,Nd@NaYF4:Nd Upconversion Nanocrystals Capped with Mn:TiO2 for 808 nm NIR-Triggered Photocatalytic Applications. Journal of Physical Chemistry C 2019, 123 (37), 22959-22970.
46. Neema, P. M.; Tomy, A. M.; Cyriac, J., Chemical sensor platforms based on fluorescence resonance energy transfer (FRET) and 2D materials. Trac-Trends in Analytical Chemistry 2020, 124.
47. Hu, Y. L.; Huang, Y.; Tan, C. L.; Zhang, X.; Lu, Q. P.; Sindoro, M.; Huang, X.; Huang, W.; Wang, L. H.; Zhang, H., Two-dimensional transition metal dichalcogenide nanomaterials for biosensing applications. Materials Chemistry Frontiers 2017, 1 (1), 24-36.
48. Li, Z. Q.; Zhang, Y., An efficient and user-friendly method for the synthesis of hexagonal-phase NaYF(4): Yb, Er/Tm nanocrystals with controllable shape and upconversion fluorescence. Nanotechnology 2008, 19 (34).
49. Wang, F.; Deng, R. R.; Liu, X. G., Preparation of core-shell NaGdF4 nanoparticles doped with luminescent lanthanide ions to be used as upconversion-based probes. Nature Protocols 2014, 9 (7), 1634-1644.
50. Lin, W.; Fritz, K.; Guerin, G.; Bardajee, G. R.; Hinds, S.; Sukhovatkin, V.; Sargent, E. H.; Scholes, G. D.; Winnik, M. A., Highly luminescent lead sulfide nanocrystals in organic solvents and water through ligand exchange with poly(acrylic acid). Langmuir 2008, 24 (15), 8215-8219.